

# Path tracking control of self-reconfigurable robot hTetro with four differential drive units

Yuyao Shi<sup>1</sup>, Mohan Rajesh Elara<sup>2</sup>, Anh Vu Le<sup>3</sup>, Veerajagadheswar Prabakaran<sup>4</sup> and Kristin L. Wood<sup>5</sup>

**Abstract**—The research interest in robots with more than one steerable wheel has been increasing over recent years due to their high mobility while having a better payload capacity than systems using omni-directional wheels. However, with more controllable degrees of freedom, almost all of the platforms include redundancy which leads to a modeling method based on the instantaneous center of rotation. The self-reconfigurable robotic platform, hTetro, is designed for floor cleaning tasks. It also has four differential-drive units which can steer individually. Differing from most other steerable wheeled mobile robots, the wheel arrangement of this robot changes because of its reconfigurability. In this paper, we proposed a robust path tracking controller that can handle discontinuous trajectories and sudden orientation changes. Singularity problems are resolved on both mechanical aspect and control aspect. The controller is tested experimentally with the self-reconfigurable robotic platform hTetro, and results are discussed.

## I. INTRODUCTION

The concept of a modular and self-reconfigurable mechanism is widely used due to its robustness, adaptability and multi-functionality. Self-reconfigurable robots are usually composed of multiple modules and able to perform shape-shifting according to different circumstances. A variety of reconfigurable systems have been developed to complete a wide range of tasks [1][2]. The system addressed in this paper is a self-reconfigurable robot developed for the floor-cleaning purpose. Inspired from the tetris game, hTetro was designed to have four modular blocks which can transform into seven configurations as shown in Fig. 1c. This enables it to access narrow spaces and increases the area coverage as proved in [3][4]. The advantages of using linked modular-type robot over multiple units are 1) the former is not limited by means of data transfer as the signals are transmitted through wires. 2) The requirement of computational power is lower for controlling one unit comparing to multiple units. Thus, with the same ability in area coverage, the platform

using linked modular-type has less requirements on the environment as well as hardware. The platform introduced in this paper is a robust version of hTetro which uses four differential drive modules and free hinges instead of mecanum wheels with actuated servo hinges [3]. By using a differential drive against four mecanum wheels in each module [3], hTetro is capable of moving on uneven terrain such as carpet or cement floor. In [3][4] the active hinge joints were used to change the configuration which results in low robustness due to servo break down. The modified design presented here uses free hinged joints. Electromagnets are used between the blocks to maintain the specific configuration during locomotion while transformation is done by decoupling electromagnets and drive the modules individually. This design helps to increase the robustness of the platform. During our three-month trial at a food court, there is no failure happened at the hinges. The detailed description of the mechanism design is presented in Section II-A.

The difficulty in controlling a robot with multiple steering modules lies upon satisfying the rigid body kinematic constraints. Lee and Tzue-Hseng proposed a kinematic and dynamic control law based on Lyapunov method and verified the stability in simulation [5]. The drawback with this method is that it does not consider the non-holonomic constraints of the platform during the modeling which in practice will lead to improper alignment of wheels. One of the disadvantages of the skidding motion is the tire wear. Since the robot with multiple steering drive is having more maneuverability than tanks and tracks, it is possible to avoid this problem. Some of the solutions are to design mechanical linkages between the wheels to prevent conflict in steering angles [6][7][8]. However, the additional mechanical linkage limits the steering angle and results in less maneuverability. It is also not suitable in this reconfigurable platform.

Modeling the platform under the instantaneous center of rotation (ICR) space is an alternative method. Although having the ICR and individual steering wheel configuration ensures the stability, there are singularity problems coping with it. The singularity happens on two aspects which are representation aspect and mathematical aspect. The former refers to the situation where the steerable wheels are parallel with each other. In this case, the ICR is theoretically located at infinity. In order to solve the representational singularity, coordinate switching is one of the proposed methods [9][10]. The latter refers to the situation where the ICR is located along the steering axes. In this case, there are more than one solutions to the desired angular velocity. This singularity has been addressed via creating artificial potential fields,

\*This work is supported by Singapore National Robotics R&D Program Office and SUTD-MIT International Design Center.

<sup>1</sup>Y. Shi is with the Department of Engineering Product Development, Singapore University of Technology and Design, 487372 Singapore, yuyao.shi@sutd.edu.sg

<sup>2</sup>M. R. Elara is with Department of Engineering Product Development, Singapore University of Technology and Design, 487372 Singapore, rajesh.mohan@sutd.edu.sg

<sup>3</sup>A. V. Le is with Optoelectronics Research Group, Faculty of Electrical and Electronics Engineering, Ton Duc Thang University, Ho Chi Minh City 700000, Vietnam, leanhvu@tdtu.edu.vn

<sup>4</sup>V. Prabakaran is with Department of Engineering Product Development, Singapore University of Technology and Design, 487372 Singapore, prabakaran@sutd.edu.sg

<sup>5</sup>K. L. Wood is the associate provost (graduate studies), Co-director of SUTD-MIT International Design Centre, Singapore University of Technology and Design, 487372 Singapore, kristinwood@sutd.edu.sg

as reported in [9][11][12] or by offsetting the steering axis outside of the wheel plane [13][14][15]. However, the usage of artificial potential field limited the position of ICR while offsetting the steering axis leads to the coupling between steering and propulsion motion. [7] Another method, proposed by Oftadeh, handles the singularity problem by addressing the maximum velocity and acceleration at the joints. In all the method proposed, the control problem is complicated either by considering the coupling between steering and propulsion motion or by involving dynamic control [16][17][18]. Other attempts were made using damped inverse kinematics schemes in [14] and [19].

In the early development of hTetro, Tun also made use of the individual steering drive mechanism [20]. Predefined-Radius-Lo-motion (PRL) and Fixed-Heading-Angle-Lo-motion (FHAL) were performed to test the maneuverability of the robot. The transformation mechanism of hTetro was also illustrated in detail. However, no path tracking control strategy and singularity avoidance were considered in the previous version. The main contributions of this paper focus on two aspects. Firstly, a mechanical design that avoid the singularity where ICR is located at the steering center. By using differential drive, the singularity problem can be avoid naturally without complicate the kinematics. Secondly, a robust path tracking controller that fits different combinations of wheel arrangement. The controller design only considers the kinematics. The framework consists of two layers of controller design: a lower level controller on the module level to ensure the kinematic constraints during transient state, and the higher level controller to determine the ICR and the corresponding steering angles.

The paper is organised into five sections. The kinematic model based on instantaneous center of rotation is derived in Section II. Section III describes the controller design and the method to avoid conflicting the kinematic constraints. Experiments with the designed hTetro and the corresponding results are presented in Section IV. Section V concludes with future works.

## II. KINEMATIC MODEL

In this section, the mechanical design and system architecture of the current hTetro platform are presented. A kinematic formulation is also developed in Section II-B which is different from that of the normal fixed morphology robot because of its reconfigurability.

### A. Robot description and modeling parameters

The platform, as shown in Fig. 1a, consists of four modules connected by three free hinges. Each of the module has a differential-drive locomotion module driven by two 12V DC motors. The locomotion modules are connected with the four chassis through the bushing on the central rod. Hence, the heading angles of the locomotion modules are independent of those of their corresponding chassis as well as that of the whole robot. With respect to electronics, we separated it as global and local peripheries. The global components such as LIDAR, IMU, and Compute stick act

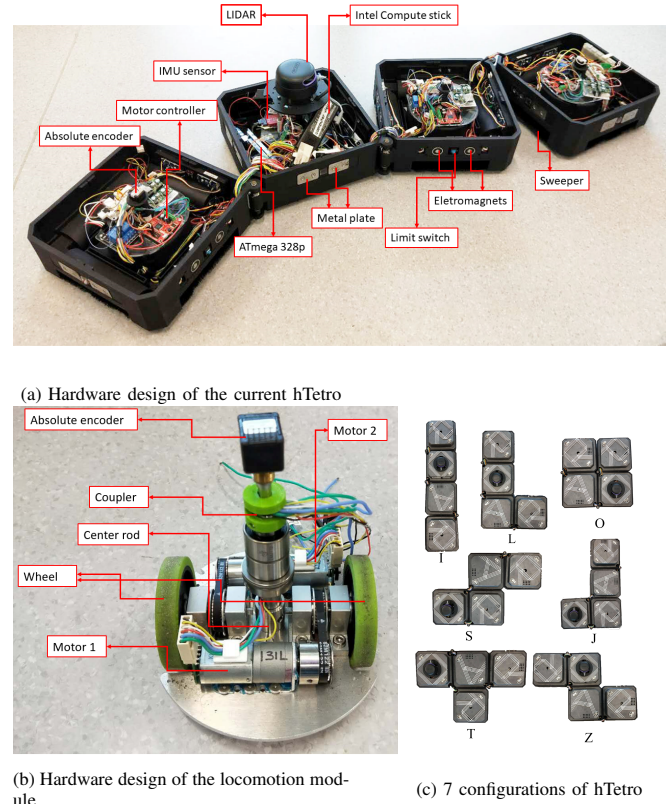


Fig. 1: Mechanical design and hardware placement

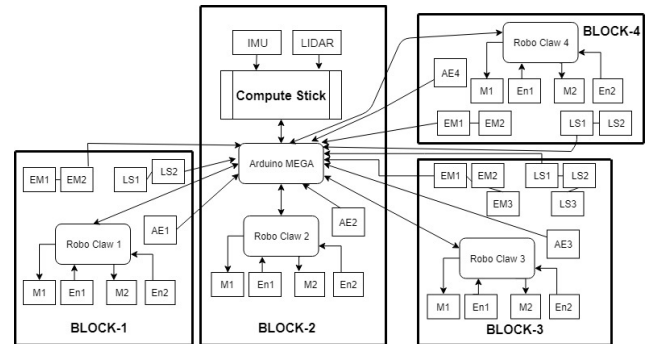


Fig. 2: hTetro System Architecture

as a top layer which helps the robot to perform SLAM, and autonomous navigation. Since block 2 acts as an anchor point for hTetro, we align the orientation of the whole robot with that of the second block. The local components such as Motor driver (roboclaw), electromagnet (EM), Limit switch (LS), absolute encoders (AE) Motors (M), and its encoders (En) would execute the reconfiguration and locomotion of hTetro. Electromagnets were used to hold the blocks position that would maintain the morphology during navigation. Limit switches were used to ensure the completion of reconfiguration and to detect the morphology failures. Except in block 2, we housed two sets in block 1, and 4 and three sets in block 3 of EM and LS components. When it comes to locomotion, we have a set of motor driver, motor, and encoder in each block. We used roboclaw motor driver to control the motors

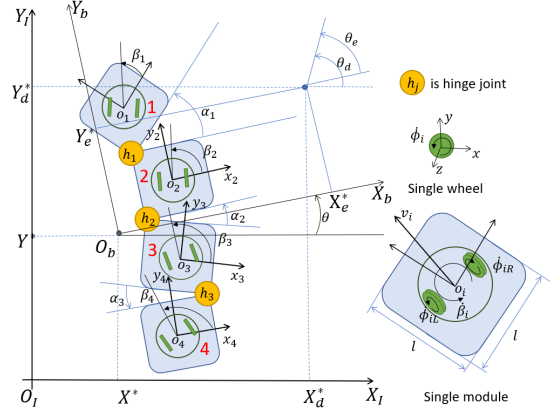
TABLE I: modeling Parameters

Symbols	Description
$\mathcal{F}_I$	World frame
$\mathcal{F}_b$	Robot frame
$X^*, Y^*$	Current position of COG w.r.t frame $\mathcal{F}_I$
$X_d^*, Y_d^*$	Desire position of COG w.r.t frame $\mathcal{F}_I$
$\theta^*$	Current orientation of the robot w.r.t frame $\mathcal{F}_I$
$\theta_d^*$	Desire orientation of the robot w.r.t frame $\mathcal{F}_I$
$\theta_e$	Orientation error
$\mathcal{F}_{bi}$	Individual frame at steering axis of $i^{th}$ module
$\beta_i$	Steering angle w.r.t chasis-fixed frame $\mathcal{F}_{bi}$
$\alpha_j$	Angle at $j^{th}$ hinge
$X_e^*, Y_e^*$	Position error under $\mathcal{F}_b$
$R$	Current instantaneous radius of rotation under $\mathcal{F}_b$
$\gamma$	Current driving angle of the robot under $\mathcal{F}_b$
$R_d$	Desire instantaneous radius of rotation under $\mathcal{F}_b$
$\gamma_d$	Desire driving angle of the robot under $\mathcal{F}_b$
$\phi_{iL}, \phi_{iR}$	rotational speed of $i^{th}$ module's left/right wheel
$v_i$	Linear velocity of $i^{th}$ module
$r_w$	Wheel radius
$d$	Wheel to center distance
$l$	Length of each module

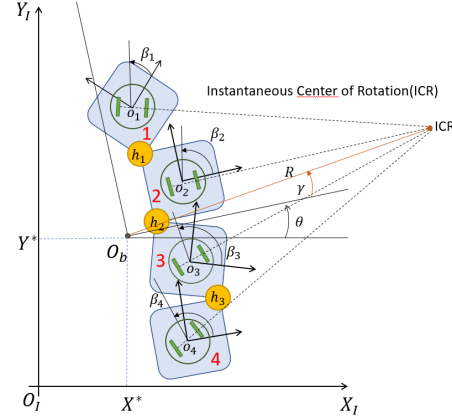
and to collect the encoder signals which would be transferred to the Local controller. On top of every locomotion module, we housed an absolute encoder (AE) that could sense the angular position and send the data back to the controller. Almost every local peripheral's data acquisition is done by the local controller for which we employed arduino MEGA that is housed in block 2. Arduino Mega is the only local components that communicates with compute stick and distributes the commands to low level peripherals to perform the tasks effectively. A detailed system architecture of the hTetro robot is shown in Fig. 2. The assumptions made during the modeling are 1)The robot does not perform shape changing during locomotion. In other words, it is treated as a rigid platform during the locomotion. 2) The wheels roll with no slipping and no skidding during the locomotion. The legends for the symbols used are described in TABLE I (see also Fig. 3):

### B. Kinematic modeling

Fig. 3 shows a schematic plot of the mobile robot under the world inertial frame. The position of the robot is defined as the position of the centroid from the top view and the orientation is defined by the orientation of LIDAR which imposes the orientation of the orientation of the chassis of the second module. Each individual module is separated from the others. So for each differential drive module, it has  $v_i = \frac{1}{2}r_w(\phi_{iL} - \phi_{iR})$  and  $\dot{\beta}_i = \frac{1}{2}r_w(\phi_{iL} + \phi_{iR})$ . Let  $\xi^* = [x^* y^* \theta^*]^T$  be the 3D task space coordinate under  $\mathcal{F}_I$  and  $\xi_d^*$  denotes the desire one. The position of the centroid of the platform  $O_b$  is defined to be  $[\frac{\sum_{i=1}^4 m_i x_i}{\sum_{i=1}^4 m_i}, \frac{\sum_{i=1}^4 m_i y_i}{\sum_{i=1}^4 m_i}]$  where  $m_i$  is the mass of each module of hTetro. By treating each locomotion module as a whole, the forward kinematics



(a) Schematic of the robot kinematic model



(b) Schematic of ICR model

Fig. 3: Schematic diagrams of hTetro.

of the robot can be expressed as:

$$\dot{\xi}^* = \mathbf{R}(\theta) \mathbf{g}(\beta_i) v_i \quad (1)$$

with  $v_i = [v_1 \ v_2 \ v_3 \ v_4]^T$  and  $\mathbf{g}^T(\beta_i) =$

$$\begin{bmatrix} \cos(\beta_1 + \alpha_1) & \sin(\beta_1 + \alpha_1) & \frac{\overrightarrow{O_b O_1}^\perp}{4||\overrightarrow{O_b O_1}||^2} \\ \cos(\beta_2) & \sin(\beta_2) & \frac{\overrightarrow{O_b O_2}^\perp}{4||\overrightarrow{O_b O_2}||^2} \\ \cos(\beta_3 + \alpha_2) & \sin(\beta_3 + \alpha_2) & \frac{\overrightarrow{O_b O_3}^\perp}{4||\overrightarrow{O_b O_3}||^2} \\ \cos(\beta_4 + \alpha_2 + \alpha_3) & \sin(\beta_4 + \alpha_2 + \alpha_3) & \frac{\overrightarrow{O_b O_4}^\perp}{4||\overrightarrow{O_b O_4}||^2} \end{bmatrix}$$

The last column of  $\mathbf{g}(\beta_i)$  is to get the orthogonal projection of  $v_i$  on the line connecting the centroid of the platform and that of each module.  $\mathbf{R}(\theta)$  is the transformation matrices from  $\mathcal{F}_b$  to  $\mathcal{F}_I$ .

In addition, with the assumption that no reconfiguration is allowed during movement,  $\dot{\theta}^*$  is defined to be the angular velocity at the centroid of the current shape which coincide with the angular velocities of all four chassis. The inverse kinematics is found through pseudo inverse of the forward kinematics.

However, as the platform is a redundant system, only using pseudo inverse to get the inverse kinematics does not ensure the kinematic constraints are fulfilled. Therefore, the actuation command of each motor is regulated with respect to

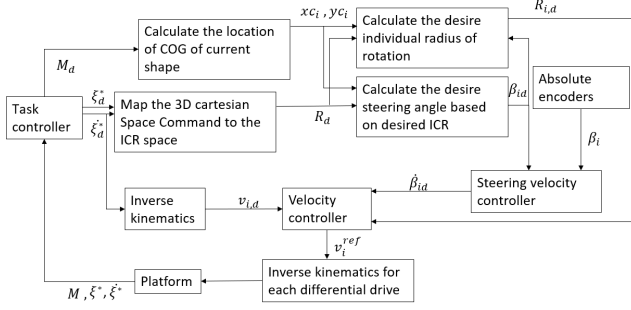


Fig. 4: Control framework of hTetro

the ICR placement which will be discussed in the following section.

### III. PATH TRACKING CONTROLLER DESIGN

In this section, the control framework for hTetro will be presented, including locating of ICR, steering angle calculation, and controller design. The schematic diagram of the control framework is shown in Fig. 4. In order to perform the cleaning task, the platform navigation is based on waypoints which contain the information of the desired position and orientation. Only when the platform reaches the waypoint correctly, the next waypoint information will be given. In between two waypoints, the center of gravity of the robot is supposed to follow a straight path while tracking the desire orientation. During the process above, the desired position and velocity \$(\xi^\*, \dot{\xi}^\*)\$ were given by a high-level perception controller and then mapped to find the desired location of instantaneous center of rotation (\$ICR\_d\$). Inspired from the previous work [10], the position of the \$ICR\_d\$ is expressed using polar coordinates assigned with \$\mathcal{F}\_b\$. The output is then used to calculate the desired corresponding steering angles (\$\beta\_{id}\$) and individual radius of rotation (\$r\_i\$). These information will be fed into the individual steering angle controller together with the current instantaneous center of rotation to determine the angular velocity \$\dot{\beta}\_{id}\$ of each steering module. After that, due to the hardware limitation of the motor, a velocity controller will be used to regulate the desired linear velocity of each module (\$v\_{id}\$) to generate the corresponding angular velocity (\$\dot{\phi}\_{iL}^{real}\$ and \$\dot{\phi}\_{iR}^{real}\$) of each wheel.

#### A. First Layer: Locating Desired Instantaneous Center of Rotation

With the given desired position \$(X\_d^\*, Y\_d^\*)\$ on the reference trajectory and current position \$(X^\*, Y^\*)\$, the error defined under robot frame is

$$\begin{bmatrix} X_e^* \\ Y_e^* \end{bmatrix} = \begin{bmatrix} \cos(\theta^*) & -\sin(\theta^*) \\ \sin(\theta^*) & \cos(\theta^*) \end{bmatrix} \begin{bmatrix} X_d^* - X^* \\ Y_d^* - Y^* \end{bmatrix} \quad (2)$$

The position error information is used to generate the angular coordinate of the desired ICR location (\$\gamma\_d\$) which is defined to be

$$\gamma_d = \arctan\left(\frac{Y_e^*}{X_e^*}\right) \quad (3)$$

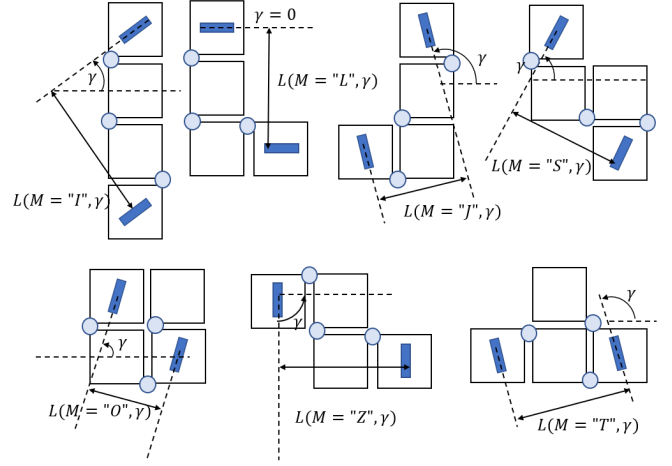


Fig. 5: Examples of \$L(M, \gamma)\$ under seven different morphology.

It indicates that when there is only error in linear position, \$\gamma\_d\$ will be the driving direction of the robot. On the other hand, when there also exists error in the orientation, the desired radius of rotation is estimated by treating the whole platform as a two-wheel-differential-drive robot. The two wheels with the maximum distance between their x-y planes are modeled to be the two wheels of the differential-drive as shown in Fig. 5 because the maximum velocity and the minimum velocity will only occur at these two modules. As the smallest curvature that a differential drive robot can achieve under certain shape is affected by the width between its two wheels, taking the two wheels with the maximum distance ensure the desired radius of the curvature does not exceed the hardware limit. Hence, the distance between the two modules is the width between the two equivalent wheels. Knowing that \$\theta\_e = \theta\_d^\* - \theta^\*\$, the desired angular velocity of the equivalent differential-drive model is controlled by a proportion controller with an adaptive gain \$\dot{\theta}\_d = k\_p \theta\_e\$.

The equivalent left wheel velocity (\$v\_l'\$) and right wheel velocity (\$v\_r'\$) for the differential-drive model are estimated by

$$\begin{cases} v_r' = \text{sign}(\dot{X}_d^*) \sqrt{\dot{Y}_d^{*2} + \dot{X}_d^{*2}} - L(M, \gamma) \dot{\theta}_d \\ v_l' = \text{sign}(\dot{X}_d^*) \sqrt{\dot{Y}_d^{*2} + \dot{X}_d^{*2}} + L(M, \gamma) \dot{\theta}_d \end{cases} \quad (4)$$

where \$L(M, \gamma)\$ refers to the perpendicular distance between the equivalent wheels under the current morphology \$M\$ with the current driving angle. Function \$\text{sign}(\dot{X}\_d^\*)\$ outputs -1 when \$\dot{X}\_d^\* < 0\$ or 1 when \$\dot{X}\_d^\* \ge 0\$ which is used to cover the two dimensional ICR space as \$\gamma\_d \in [-\frac{\pi}{2}, \frac{\pi}{2}]\$. Therefore, the instantaneous radius of rotation derived from (4) can be represented as

$$R_d = \frac{L(M, \gamma)}{2} \frac{v_l' + v_r'}{v_l' - v_r'} = \frac{\text{sign}(\dot{X}_d^*) \sqrt{\dot{Y}_d^{*2} + \dot{X}_d^{*2}}}{\dot{\theta}_d} \quad (5)$$

However, as there is obvious singularity when \$\dot{\theta}\_d = 0\$ in (5), an alternative method to constrain the radius is proposed below using hyperbolic tangent function with a big

enough value  $R_{max}$  considering the computational speed and resolution of the absolute encoders.

$$R_d = R_{max} \tanh\left(\frac{\sqrt{\dot{Y}_d^{*2} + \dot{X}_d^{*2}}}{\dot{\theta}_d R_{max}}\right) \quad (6)$$

The location of  $ICR_d$  under  $\mathcal{F}_b$  is defined by the desired tangential driving angle  $\gamma_d$  and the radius  $R_d$  which separates the linear motion and the angular motion of hTetro. It allows hTetro platform to correct either of the attributes while maintaining the other.

### B. Second Layer: Individual Steering Velocity Controller

The hTetro is able to change to seven different shapes and the relative position of each locomotion module also changes. The position of the steering axes with respect to  $\mathcal{F}_b$  are denoted as  $(x_i^c, y_i^c)$  with  $i \in \{1, 2, 3, 4\}$ . After that, the desired steering angle  $(\beta_{i,d})$  and individual instantaneous radius of rotation  $(r_i)$  of each module can be represented as

$$\beta_{i,d} = \arctan\left(\frac{y_i^c - R_d \sin(\gamma_d)}{R_d \cos(\gamma_d) - x_i^c}\right) - \alpha_j \quad (7)$$

$$r_i = \frac{y_i^c - R_d \sin(\gamma_d)}{\sin(\beta_{i,d})} \quad (8)$$

$$\text{while } \alpha_j = \begin{cases} \alpha_1 & i = 1 \\ 0 & i = 2 \\ \alpha_2 & i = 3 \\ \alpha_2 + \alpha_3 & i = 4 \end{cases}$$

Because the control signals  $\dot{\beta}_{i,d}$  are error driven, when discontinuous signal is given, for instance, when the robot arrived at the waypoint, it is likely that the required motor speed exceeds its hardware limit. Hence, a constrained feedback controller is used to regulate the linear velocities  $(v_i)$  which will be illustrated in Section III-C. From the absolute encoder, as shown in Fig. 1b, the current steering angle of each locomotion module  $(\beta_i)$  is used to compare the difference. On top of that, the initial steering angles are initialized according to the initial  $ICR_d$ . The desired steering velocities are controlled according to the steering error  $\beta_{i,e} = \beta_{i,d} - \beta_i$  such that the kinematic constraint will be fulfilled during the transition period. In other words, the controller is used to ensure the lines co-linear with the radii as expressed in (9) are always concurrent when  $v_i \neq 0$  because the four locomotion modules are indifferent when  $v_i = 0$ . The  $\alpha_j$  used in (9) are defined the same way as (7).

$$-\frac{1}{\tan(\beta_i + \alpha_j)}(x - x_i^c) = (y - y_i^c) \quad (9)$$

(9) can be written in the form  $\mathbf{A}\mathbf{x} = \mathbf{b}$  where  $\mathbf{x} = [x \ y]^T$  and  $\mathbf{A}$  is the coefficient matrix of the individual radius of rotation. Then, its augmented matrix

$$[\mathbf{A}|\mathbf{b}] = \left[ \begin{array}{cc|cc} \frac{-1}{\tan(\beta_1 + \alpha_1)} & -1 & \frac{-1}{\tan(\beta_1 + \alpha_1)}x_1^c + y_1^c & \\ \frac{-1}{\tan(\beta_2)} & -1 & \frac{-1}{\tan(\beta_2)}x_2^c + y_2^c & \\ \frac{-1}{\tan(\beta_3 + \alpha_2)} & -1 & \frac{-1}{\tan(\beta_3 + \alpha_2)}x_3^c + y_3^c & \\ \frac{-1}{\tan(\beta_4 + \alpha_2 + \alpha_3)} & -1 & \frac{-1}{\tan(\beta_4 + \alpha_2 + \alpha_3)}x_4^c + y_4^c & \end{array} \right] \quad (10)$$

TABLE II: Relationships among  $x_i^c$  or  $y_i^c$

shape	$x_i^c$ relationship	$y_i^c$ relationship
I	$x_1^c = x_2^c = x_3^c = x_4^c = 0$	$y_1^c = 3y_2^c = -3y_3^c = -y_4^c$
L	$x_1^c = x_2^c = x_3^c = -x_4^c$	$y_1^c = 3y_2^c = -3y_3^c = y_4^c$
Z	$x_1^c = x_4^c, x_2^c = x_3^c = 0$	$y_1^c = y_2^c = -y_3^c = -y_4^c$
O	$x_1^c = x_2^c = -x_3^c = -x_4^c$	$y_1^c = -y_2^c = -y_3^c = y_4^c$
T	$x_1^c = -3x_2^c = x_3^c = x_4^c$	$y_1^c = -y_4^c, y_2^c = y_3^c = 0$
S	$x_1^c = x_3^c = 0, x_2^c = -x_4^c$	$y_1^c = y_2^c = -y_3^c = -y_4^c$
J	$-x_1^c = x_2^c = x_3^c = x_4^c$	$y_1^c = y_2^c = -3y_3^c = -y_4^c$

With the initialization of the steering angles, it is known that  $\text{rank}(\mathbf{A}_{init}|\mathbf{B}_{init}) = \text{rank}(\mathbf{A}_{init}) \leq 2$  which means all four lines that are co-linear with radii are either parallel or concurrent. Similarly, we also know that at the final state all the steering angles should fulfill the kinematic constraint which indicates that  $\text{rank}(\mathbf{A}_d|\mathbf{B}_d) = \text{rank}(\mathbf{A}_d) \leq 2$ . Hence, these two situations will be illustrated separately in Section III-B.1 and Section III-B.2.

#### 1) Both initial state and desired state are parallel:

Under this situation,  $\dot{\theta}_d = 0$  and  $\beta_{i,e} = \gamma_d - \gamma$  which means the robot only perform translational motion. The ranks of the coefficient and augmented matrices are one. Therefore, the steering velocity profiles of all four modules should be the same. In this case, a PID controller was used to keep the heading angle unchanged. Therefore,  $\dot{\beta}_i(t) = k_p \gamma_e(t) + k_i \int_0^t \gamma_e(t) dt + k_d \frac{d\gamma_e(t)}{dt}$ . As the initial state with an arbitrary  $\gamma$  could satisfy the constraint, substituting  $\beta_i$  with  $\beta_i + \int_0^t \dot{\beta}_i(t) dt$  will not violate the constraint as well.

2) Either initial state or desired state is concurrent: When the initial or final state is concurrent, the solution for the system is unique, indicating ranks of both matrices are two. By doing row-echelon reduction and rearranging the column of the the augmented matrix, matrix  $\mathbf{A}$  and vector  $\mathbf{b}$  can be express as (11).

$$\mathbf{A} = \begin{bmatrix} 1 & \frac{1}{\tan(\beta_1 + \alpha_1)} \\ 0 & \frac{1}{\tan(\beta_2)} - \frac{1}{\tan(\beta_1 + \alpha_1)} \\ 0 & \frac{1}{\tan(\beta_3 + \alpha_2)} - \frac{1}{\tan(\beta_1 + \alpha_1)} \\ 0 & \frac{1}{\tan(\beta_4 + \alpha_2 + \alpha_3)} - \frac{1}{\tan(\beta_1 + \alpha_1)} \end{bmatrix} \quad (11)$$

$$\mathbf{b} = \begin{bmatrix} \frac{1}{\tan(\beta_1 + \alpha_1)}x_1^c + y_1^c \\ \frac{1}{\tan(\beta_2)}x_2^c - \frac{1}{\tan(\beta_1 + \alpha_1)}x_1^c + y_2^c - y_1^c \\ \frac{1}{\tan(\beta_3 + \alpha_2)}x_3^c - \frac{1}{\tan(\beta_1 + \alpha_1)}x_1^c + y_3^c - y_1^c \\ \frac{1}{\tan(\beta_4 + \alpha_2 + \alpha_3)}x_4^c - \frac{1}{\tan(\beta_1 + \alpha_1)}x_1^c + y_4^c - y_1^c \end{bmatrix} \quad (12)$$

Due to the geometry property of the seven configurations, the relationship among all  $x_i^c$  or among  $y_i^c$  are summarized in TABLE II.

As a result, by substituting the relationships in TABLE II to (11), it can be found that the following relationship between the steering angles should be fulfilled.

$$\frac{1}{\tan(\beta_1 + \alpha_1)} - C_1 \frac{1}{\tan(\beta_2)} - C_2 \frac{1}{\tan(\beta_3 + \alpha_2)} - C_4 \frac{1}{\tan(\beta_4 + \alpha_2 + \alpha_3)} = 0 \quad (13)$$



The relationship above is derived by assuming the system is consistent.  $C_i$  are constant coefficient for different shapes with respect to TABLE.II. Due to the assumption made in Section II-B, the relationships among  $x_i^c$  and  $y_i^c$  will not change during locomotion. Thus, in order to fulfill the concurrent requirement,  $\dot{\beta}_i(t)$  should be restricted by the following criteria

$$\int_0^T \dot{\beta}_i(t)dt = \beta_{i,e} \quad (14)$$

to ensure it reaches the desired angle at the same time instance, and

$$\tan(\beta_{i,init} + \int_0^t \dot{\beta}_i(t)dt + \alpha_j) = \lambda \tan(\beta_{i,init} + \alpha_j) \quad (15)$$

or

$$\tan(\beta_{i,init} + \int_0^t \dot{\beta}_i(t)dt + \alpha_j) = \lambda \tan(\beta_{i,d} + \alpha_j) \quad (16)$$

to ensure the kinematic constraint depending on the concurrent state.

Starting from initialization,  $\dot{\beta}_i^+$  is defined to be the desired velocity of the first time instance.

$$\beta_i^+ = \int_0^{t^+} \dot{\beta}_i^+ dt \quad (17)$$

Substitute (17) into (14),

$$\beta_{i,e}^+ = \beta_{i,e} - \beta_i^+ \quad (18)$$

$$\tan(\beta_{i,init} + \beta_i^+ + \alpha_j) = \frac{\tan(\beta_{i,init} + \alpha_j) + \tan(\beta_i^+)}{1 - \tan(\beta_{i,init} + \alpha_j) \tan(\beta_i^+)} \quad (19)$$

Hence,

$$\lambda = \frac{1 + \frac{\tan(\beta_i^+)}{\tan(\beta_{i,init} + \alpha_j)}}{1 - \tan(\beta_i^+)} \quad (20)$$

or

$$\lambda = \frac{1 + \frac{\tan(\beta_i^+)}{\tan(\beta_{i,d} + \alpha_j)}}{1 - \tan(\beta_i^+)} \quad (21)$$

In order to ensure the linear dependency is followed by all four module,  $\lambda$  is defined by substituting the maximum  $\dot{\beta}_i$  in to (17) which is determined by the maximum  $\beta_{i,e}$  to fulfill criteria (14) through a PID controller. Thus, the module with the maximum error will be used as reference to calculate the  $\lambda$ . After that, the rest of the steering angles ( $\beta_i^+$ ) are calculated based on (21) which is then used to determine the steering speed of the rest modules ( $\dot{\beta}_i$ ).

### C. Constraint Individual Velocity Controller

According to Section III, a constraint velocity controller need to be implemented to restrict the maximum drive rate of each motor. Referring to (8) and (5), the desired linear velocity of each module can be expressed as

$$v_{id} = \frac{r_i}{R_d} \sqrt{\dot{Y}_d^{*2} + \dot{X}_d^{*2}} = \frac{r_i}{R_d} \dot{\theta}_d = \frac{r_i}{R_d} k_p (\theta_d - \theta) \quad (22)$$

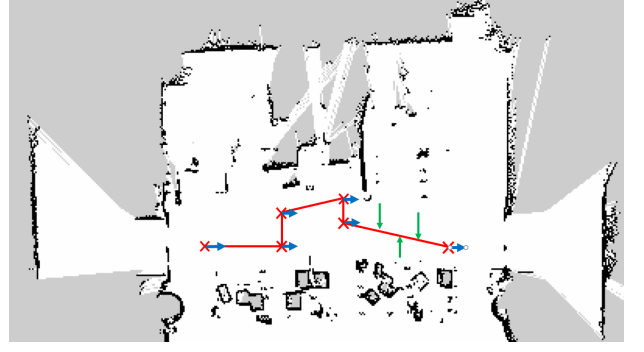


Fig. 6: 2D map used for the experiment

the desired drive rate of each motor is

$$\dot{\phi}_{iL} = \frac{\dot{\beta}_i}{r_w} + \frac{\dot{v}_{id}}{r_w} \quad (23)$$

$$\dot{\phi}_{iR} = \frac{\dot{\beta}_i}{r_w} - \frac{\dot{v}_{id}}{r_w} \quad (24)$$

Substituting (22) into (23),

$$\dot{\phi}_{iL} = \frac{\dot{\beta}_i}{r_w} + \frac{r_i}{R_d} k_p \frac{(\theta_d - \theta)}{r_w} \quad (25)$$

$$\dot{\phi}_{iR} = \frac{\dot{\beta}_i}{r_w} - \frac{r_i}{R_d} k_p \frac{(\theta_d - \theta)}{r_w} \quad (26)$$

In order for the drive rate not to exceed the drive limit  $\dot{\phi}_{max}$  according to the hardware limitation of the motor,  $k_p$  is determined by limiting the larger velocity between (19) and (20) to  $\dot{\phi}_{max}$ .

$$k_p = \frac{r_w \min\{\dot{\phi}_{max}, \max\{\dot{\phi}_{iL}, \dot{\phi}_{iR}\}\} - \dot{\beta}_i}{\frac{r_i}{R_d} (\theta_d - \theta)} \quad (27)$$

where the max function is used to extract the maximum desired drive rate among all eight motors and the min function is used to compare it with the limit. After determining the gain value, the real driving command  $\dot{\phi}_{iL}^{real}$  and  $\dot{\phi}_{iR}^{real}$  can be obtained by substituting the  $k_p$  into (25) which will be fed into the platform.

## IV. EXPERIMENT AND RESULT

In this section, the experimental setup with explanation is presented in detail, together with the result and discussion. The experiment was done using the hTetro platform as shown in Fig. 1. Fig. 6 shows the 2D map used for the experiment. The waypoints set for the robot are marked by red crosses. The green arrows indicate the points when external disturbances are introduced and the blue arrows are to show the desired orientation. As all seven shapes of the robot are governed by the same kinematic model, the experiments were only done with 'O' shape.

In order to test it in the real scenario, only waypoints containing the desired position and orientation are given to the robot. The waypoints are set to make the robot perform the zig-zag pattern and diagonal motion while keeping the

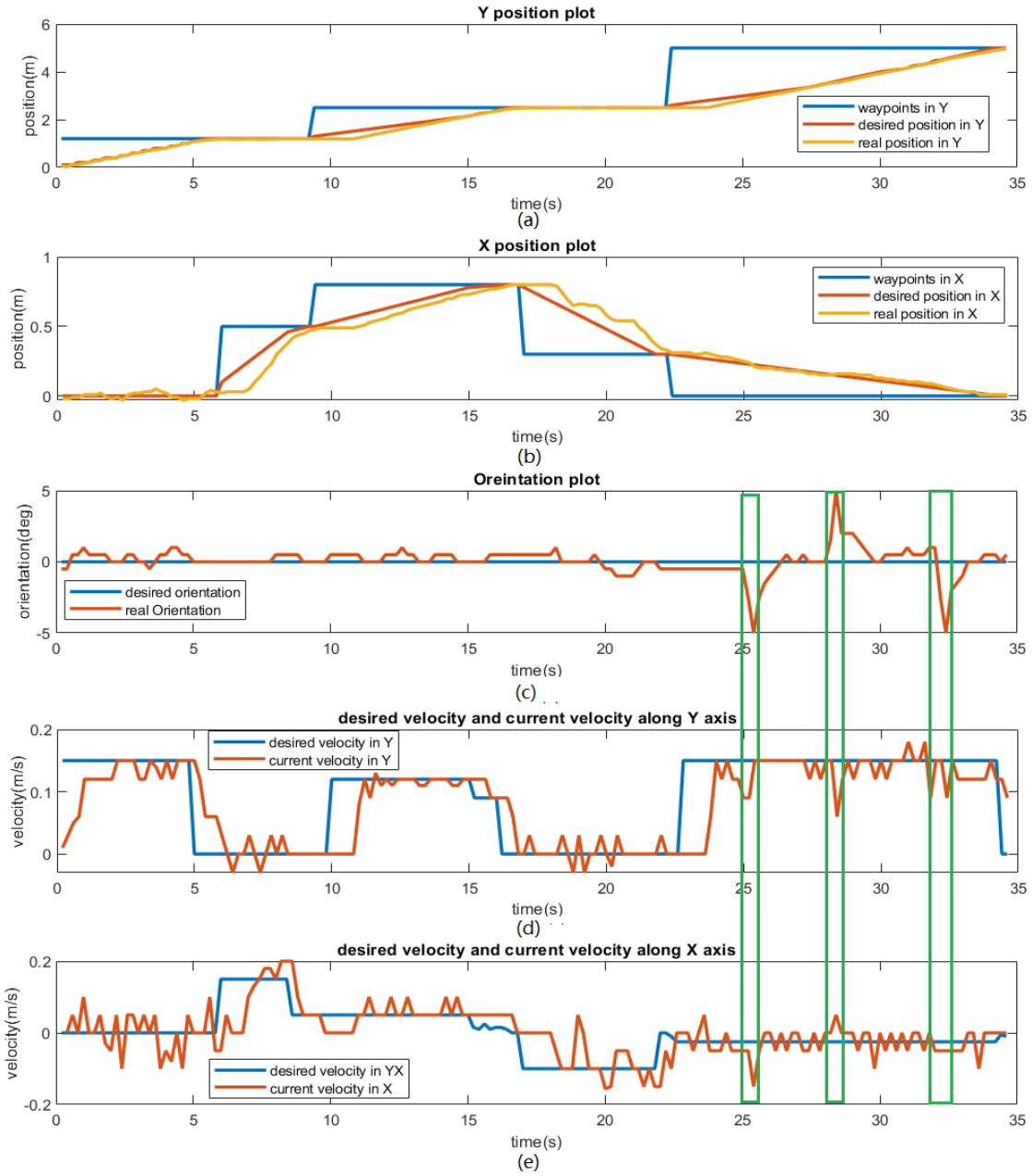


Fig. 7: Results of the proposed controller under Cartesian space. (a) Position: Waypoints, desired position and real position in Y. (b) Position: Waypoints, desired and real position in X. (c) Orientation: Desired and real orientation. (d) Velocity: Desired and real velocity along Y. (e) Velocity: Desired and real velocity along X.

orientation and steering angles with the controller proposed above. Sequences of the waypoints received by the robot are  $(0, 1.2)$ ,  $(0.5, 1.2)$ ,  $(0.8, 2.5)$ ,  $(0.3, 2.5)$ , and  $(0, 5)$  with all dimensions measured in meters. Disturbances are given to the robot by kicking on its side. The result of the experiments are shown in Fig. 7. The waypoints are discontinuous locations on the map and the desired position is determined using the integration of the desired speed. As for the orientation, the goal is to keep track of the orientation under disturbances. The time instances when the disturbances were introduced

by the external kicking actions are depicted in Fig. 7 in green boxes.

As shown in the plots, the platform demonstrated the ability to follow the desired trajectory based on discrete waypoints and velocity commands under the Cartesian space. From the data collected, the root mean square errors of the positions in  $X$  and  $Y$  are implicitly 0.108 and 0.0623 which indicate the accurate path tracking ability of the robot. In addition, we can observe from the graph that the robot is able to overcome disturbances in different directions.

Due to the separation of the linear motion and angular motion, the orientation can be maintained and corrected without minor influence to the linear motion. However, when implementing the control strategy on the platform, some overshoot and oscillation response can be observed especially in the velocity plot. The first reason we suspected is the joggle of the robot chassis which resulted in shake of the LIDAR. Secondly, imperfect tuning parameters of the embedded motor controller might be another reason that would result in the oscillation in velocity plot. These two issues are technical problems related to the fabrication of the platform. Another reason we suspected is that of mechanical design. As we replaced the individual steering drive module with differential drive module, though it helps to weave out the singularity at the steering axis, the steering axis also becomes unactuated. As a result, the steering angle of each module is likely to be affected by the unevenness of the terrain and the desynchronization of motor speed.

## V. CONCLUSIONS

In this paper, we presented the kinematic modeling and path tracking controller design of a novel modular reconfigurable cleaning robot with usage of four differential-drive modules. The usage of differential drive to replace individual steering drive helps to avoid the kinematic singularity. Kinematics modeling was done considering the shape-shifting factor of the robot. The mapping of the ICR location enables the robot able to separate the linear and angular motion under Cartesian space. Additionally, the velocity controllers regulate the kinematic and hardware constraints of the platform making it able to fulfill the kinematic constraints under transition period. Experiments were performed under the real working scenario. The results reflect the ability of trajectory following and fast recovery from disturbances. Future research will focus on: (1) improvement on the robustness of platform; (2) dynamic controller design considering the influence of the cleaning brush.

## REFERENCES

- [1] Y. Fei and C. Wang, "Self-repairing algorithm of lattice-type self-reconfigurable modular robots," *Journal of Intelligent & Robotic Systems*, vol. 75, pp. 193–203, Aug 2014.
- [2] V. Singh, S. M. Skiles, J. E. Krager, K. L. Wood, D. Jensen, and R. Sierakowski, "Innovations in Design Through Transformation: A Fundamental Study of Transformation Principles," *Journal of Mechanical Design*, vol. 131, 07 2009.
- [3] P. Veerajagadheswar, M. R. Elara, T. Pathmakumar, and V. Ayyalusami, "A tiling-theoretic approach to efficient area coverage in a tetris-inspired floor cleaning robot," *IEEE Access*, vol. 6, pp. 35260–35271, 2018.
- [4] V. Prabhakaran, M. R. Elara, T. Pathmakumar, and S. Nansai, "htetro: A tetris inspired shape shifting floor cleaning robot," in *2017 IEEE International Conference on Robotics and Automation (ICRA)*, pp. 6105–6112, May 2017.
- [5] M. Lee and T. S. Li, "Kinematics, dynamics and control design of 4w4w mobile robots," *The Journal of Engineering*, vol. 2015, no. 1, pp. 6–16, 2015.
- [6] T. L. Lam, H. Qian, and Y. Xu, "Omnidirectional steering interface and control for a four-wheel independent steering vehicle," *IEEE/ASME Transactions on Mechatronics*, vol. 15, pp. 329–338, June 2010.
- [7] M. A. Vilaplana, O. Mason, D. Leith, and W. Leithead, "Control of yaw rate and sideslip in 4-wheel steering cars with actuator constraints," vol. 3355, pp. 201–222, 01 2003.
- [8] Z. Lu, M. Lin, S. Wang, Y. Zhang, and Y. Yu, "Research on a new-style under-actuated omnidirectional mobile robot based on special coupling drive system," *IEEE Access*, vol. 7, pp. 152138–152148, 2019.
- [9] C. P. Connette, C. Parltz, M. Hagele, and A. Verl, "Singularity avoidance for over-actuated, pseudo-omnidirectional, wheeled mobile robots," in *2009 IEEE International Conference on Robotics and Automation*, pp. 4124–4130, May 2009.
- [10] C. Connette, M. Hagele, and A. Verl, "Singularity-free state-space representation for non-holonomic, omnidirectional undercarriages by means of coordinate switching," in *2012 IEEE/RSJ International Conference on Intelligent Robots and Systems*, pp. 4959–4965, Oct 2012.
- [11] A. Dietrich, T. Wimbck, A. Albu-Schffer, and G. Hirzinger, "Singularity avoidance for nonholonomic, omnidirectional wheeled mobile platforms with variable footprint," in *2011 IEEE International Conference on Robotics and Automation*, pp. 6136–6142, May 2011.
- [12] C. P. Connette, A. Pott, M. Hagele, and A. Verl, "Addressing input saturation and kinematic constraints of overactuated undercarriages by predictive potential fields," in *2010 IEEE/RSJ International Conference on Intelligent Robots and Systems*, pp. 4775–4781, Oct 2010.
- [13] M. Sorour, A. Cherubini, P. Fraisse, and R. Passama, "Motion discontinuity-robust controller for steerable mobile robots," *IEEE Robotics and Automation Letters*, vol. 2, pp. 452–459, April 2017.
- [14] M. Sorour, A. Cherubini, R. Passama, and P. Fraisse, "Kinematic modeling and singularity treatment of steerable wheeled mobile robots with joint acceleration limits," in *2016 IEEE International Conference on Robotics and Automation (ICRA)*, pp. 2110–2115, May 2016.
- [15] M. Sorour, A. Cherubini, A. Khelloufi, R. Passama, and P. Fraisse, "Complementary-route based icr control for steerable wheeled mobile robots," *Robotics and Autonomous Systems*, vol. 118, pp. 131 – 143, 2019.
- [16] R. Oftadeh, R. Ghabcheloo, and J. Mattila, "Time optimal path following with bounded velocities and accelerations for mobile robots with independently steerable wheels," in *2014 IEEE International Conference on Robotics and Automation (ICRA)*, pp. 2925–2931, May 2014.
- [17] V. Pitknen, A. Tikanmki, A. Kemppainen, and J. Rning, "Path following controller for planar robots with articulated, actuated and independently steerable velocity-limited wheels," in *2017 IEEE International Conference on Robotics and Automation (ICRA)*, pp. 2433–2440, May 2017.
- [18] C. Stger, A. Mueller, and H. Gattringer, "Dynamic model-based control of redundantly actuated, non-holonomic, omnidirectional vehicles," pp. 69–78, 01 2016.
- [19] C. Stger, A. Mller, and H. Gattringer, "Kinematic analysis and singularity robust path control of a non-holonomic mobile platform with several steerable driving wheels," in *2015 IEEE/RSJ International Conference on Intelligent Robots and Systems (IROS)*, pp. 4140–4145, Sep. 2015.
- [20] T. T. Tun, L. Huang, R. E. Mohan, and S. G. H. Matthew, "Four-wheel steering and driving mechanism for a reconfigurable floor cleaning robot," *Automation in Construction*, vol. 106, p. 102796, 2019.